Journal of the Energy Institute 102 (2022) 206–215

Contents lists available at ScienceDirect

Journal of the Energy Institute

journal homepage: www.elsevier.com/locate/joei

Combustion instability of ethanol and n-heptane fuels under different combustor geometries

Zihua Liu, Dongliang Wei, Mengting Ji, Hao Fang, Hao Zhou *

State Key Laboratory of Clean Energy Utilization, Zhejiang University, Zheda Road 38, Hangzhou, 310027, China

ARTICLE INFO

Keywords:
Combustion instability
Ethanol
n-heptane
Oscillation

ABSTRACT

Combustion instability has become one of the most significant challenges faced in designing modern industrial gas turbines and aero-engines. In this study, the influence of combustor structure on the combustion instability of ethanol and n-heptane is explored by adjusting the plenum length (200–550 mm) and the swirler vane angle (60° and 75°). The ethanol combustion instability maps show that the oscillation frequency increases as the equivalence ratio and plenum length decrease with the stabilization range of n-heptane being broader. The maximum pressure pulsation amplitudes of ethanol and n-heptane during combustion instabilities are close to 495 and 415 Pa, respectively. The flow field temperature measurements show that the fuel properties change the flame shape and temperature distribution in the combustor, thus potentially affecting the intensity of the oscillations. Short, compact ethanol flames and more uneven temperature distribution are more likely to lead to unstable combustion. This work provides more experimental observations on the effects of fuel properties and combustion configuration on combustion stability.

1. Introduction

In order to reduce NOx emissions, industrial gas turbine manufacturers are developing lean combustion technologies [1]. However, lean fuel combustion systems are more prone to cause self-excited combustion oscillations caused by the interaction between heat release, sound and combustor geometry [2,3]. When combustion instability occurs, the phase difference between the sound pressure fluctuation p' and the heat release fluctuation Q' is less than 90° [2]. Combustion instabilities can result in vibrations and noise, shorten the service life of the equipment and cause accidental flame quenching or flashback [4,5]. In many previous works, the flame transfer or describing functions (FTFs or FDFs) were used to study the flame response to velocity or pressure fluctuations under external acoustic forcing [6]. However, spray combustion instability is also related to fuel atomization and evaporation, droplet distribution and spray movement [7]. When the combustion chamber structure or conditions change, the accuracy of the prediction results based on the FTF/FDF method decreases [8]. Although combustion instability could be weakened by installing acoustic dampers on the problematic combustors [9–12], it is even more critical to avoid oscillations in the early design phase [13].

The combustor geometry, such as length and inner diameter, is usually related to flame speed, oscillation mode, and frequency [14,15]. Gejji et al. [16] studied the effects of the chamber and plenum lengths, inlet-air temperature, equivalence ratio, nozzle position and liquid fuel composition on the self-excited combustion instabilities, and reported whether the pressure wave in the combustor was the 3/8- or half-wave mode depending on the combustor structure. The change in the equivalence ratio caused a change in the gas temperature, changing the oscillation frequency observed during the test. The oscillation frequency was low when the combustion chamber was long. Ahn et al. [17] studied the low-frequency combustion dynamics in more detail and found that the plenum length does not determine the frequency of Helmholtz-type instability. However, the longer the length of the chamber, the lower the oscillation frequency. In addition, a lower inlet-air temperature has been found to cause greater instability.

The dependence of the oscillation frequency and normalized pressure amplitude on the combustion chamber length was investigated by Lee et al. [18]. The combustion chamber length was found to have minimal effect on the oscillation frequency of a dual swirl flame but significantly changed the thermoacoustic oscillation amplitude. Through experiments, Yoon et al. [19] proved that the combustor length affects the amplitude of the pulsating pressure. Under high instability conditions, the flame shape changes drastically and the heat release rate fluctuates heavily. Xu et al. [20] found that for the quarter-wave mode,

* Corresponding author.
E-mail address: zhouhao@zju.edu.cn (H. Zhou).

https://doi.org/10.1016/j.joei.2022.03.002
Received 2 February 2022; Received in revised form 3 March 2022; Accepted 7 March 2022
Available online 23 March 2022

Nomenclature

R_i	inner radius of the primary air passage, [m]
R_o	outer radius of the primary air passage, [m]
L_p	plenum length, [m]
p	dynamic pressure, [Pa]
Q	heat release rate, [W]
S_n	geometric swirl number
Φ	equivalence ratio
ψ	installation angle of the swirler blades, [°]

the longer the chamber length, the lower the oscillation frequency. Unlike the quarter-wave mode, the intrinsic thermoacoustic (ITA) mode was insensitive to the chamber length variation and its frequency was mainly determined by the time delay of the flame response. The added bias flow had a positive effect on suppressing the quarter-wave mode instability but did not affect the ITA mode.

Furthermore, Rao et al. [21] studied the effect of combustion chamber length and equivalence ratio on combustion stability. The permutation entropy and proper orthogonal decomposition methods were demonstrated to effectively distinguish the stable state and limit-cycle oscillation, even for combustors with different lengths. Using large eddy simulations, Chen et al. [22] found that the acoustic impedance of the swirler could cause periodic variations in the mass flow rate, which led to periodic changes in the mixing and heat release rates, as well as amplifying the combustion oscillations.

Swirl number oscillations can also induce flame angle fluctuations and instabilities. Schiavo et al. [23] found that the acoustic characteristics of the swirler affected the oscillation intensity. Yi et al. [24] also reported that the swirler had an effect on the combustion stability. While the change in the vortex shear layer angle caused a significant change in the flame structure, more vigorous gas expansion promoted vortex rupture and gas recirculation, which improved the fuel and air mixing. The influence of swirl number on FTF was investigated by Durox et al. [25]. As the blade angle decreased, the flame moved downstream and the reaction zone became less compact. Precessing vortex core occurred when the swirl number exceeded 0.45. Changing the vane angle and the corresponding swirl number makes it possible to change the flame from

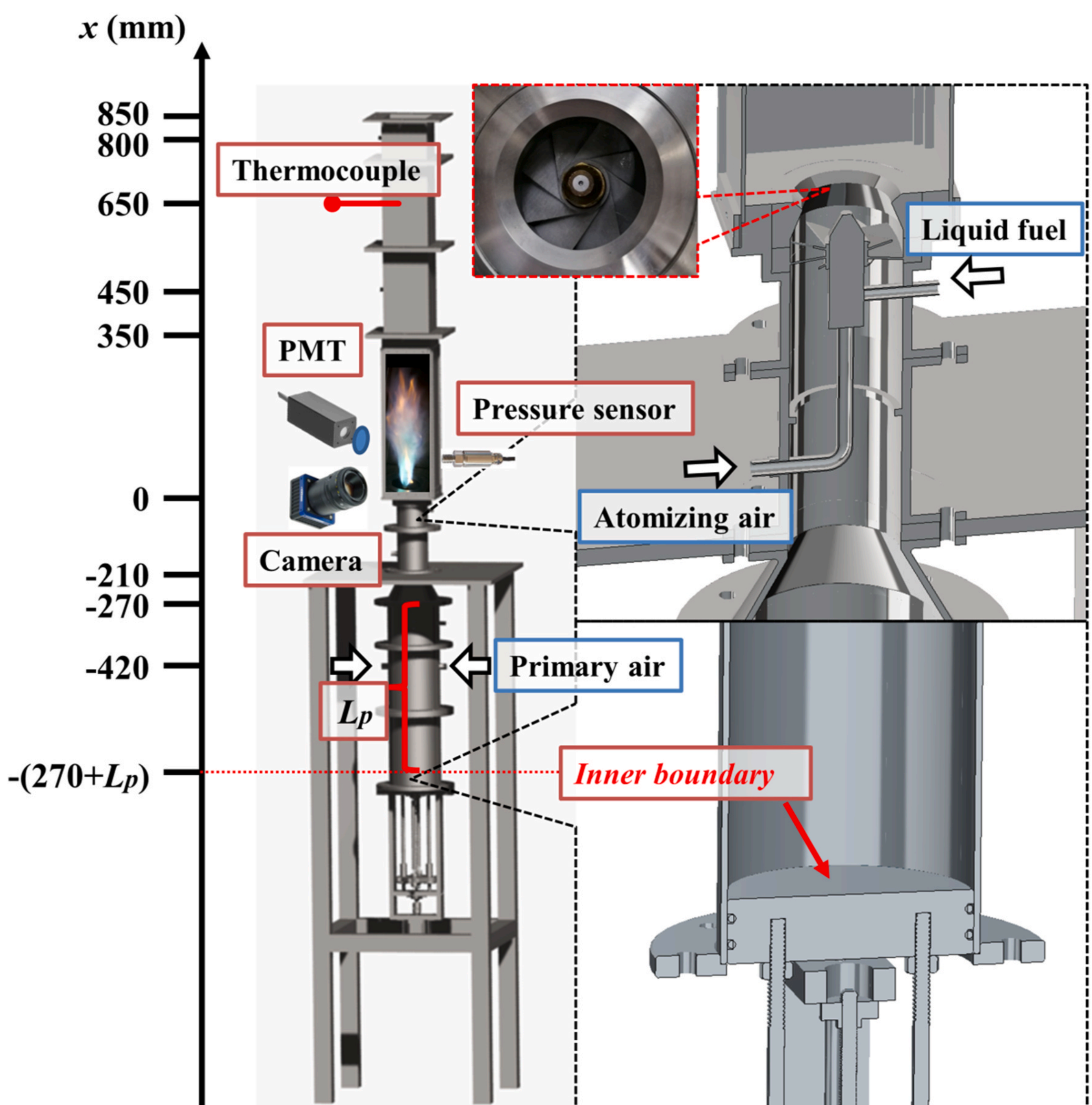

Fig. 1. Schematic diagram of the lab-scale liquid fuel and measurement equipment.

an unsteady state to a steady state. Zhang et al. [26] studied the thermoacoustic instability driving factors and mode conversion in a methane-air combustor under various swirling intensities. As the vortex intensity increased, the lateral recirculation zone and the coherent structure played a major role in causing excitation fluctuations, while the central recirculation zone had the most negligible effect on driving thermoacoustic instability.

Fuel characteristics, such as ignition delay time, also affect the combustion stability [27,28]. Soundararajan et al. [29] established instability maps of three types of liquid fuels (propane, heptane and dodecane) by changing the equivalence ratio and thermal power. Under the same operating conditions, the magnitude and frequency of the instability depended on the fuel injection conditions and fuel type. Dodecane, which has poor volatility and a long lag time, was the most stable. Karlis et al. [30] studied the influence of the inert diluents in the fuel mixture on the dynamic state of a swirl stabilized combustor. As the molar fraction of nitrogen dilution increased, the velocity oscillation amplitude of the standing wave decreased. Speth et al. [31] investigated the combustion kinetics of CO–H_2 mixtures in a syngas combustor and showed that the interaction of the flame and flow field determined the stability. When sufficient hydrogen was mixed into the fuel, the combustion became unstable and the flame became compact. The analysis showed that the quarter- and three quarter-wave modes could be excited when the equivalence ratio was close to 0.45.

In summary, the plenum length affects the oscillation frequency and intensity, the geometric swirl number affects the flame lift-off length, and the physical properties of the liquid fuel affect the heat release process. However, the combustion instability mechanism of liquid fuel, especially under different combustor structures, is not very clear [32]. This study aims to evaluate the influence of liquid fuel physical properties and combustor structure on combustion stability. Ethanol and n-heptane are volatile and relatively clean and were therefore used in this study [33,34]. Another reason for choosing ethanol and n-heptane as research fuels is that these two fuels are relatively inexpensive, renewable, readily available, and the fuel properties have been extensively studied [35,36]. Ethanol and n-heptane were chosen as research fuels because these two fuels are relatively inexpensive, renewable, readily available, and the fuel properties have been extensively studied.

To the best of the authors' knowledge, this is the first time that the effect of combustor structure on self-excited combustion instability has been explored by varying the plenum length and the installation angle of the swirler blades.

This study is structured as follows. Section 2 shows the experimental facilities and gives the operational conditions. The instability maps when burning ethanol and n-heptane are in Section 3.1 and 3.2, respectively. The length of the plenum, the installation angle of the swirler blades and the equivalence ratio are all independent variables. By measuring the axial flow field temperature and taking snapshots of the flames, the influence of the temperature distribution characteristics on the self-excited combustion instability is then analyzed in Section 3.3. The findings of this study are summarized in Section 4.

2. Experimental setup and procedures

The investigations were performed on a lab-scale liquid-fueled combustor, including a plenum, a siphon type air atomizing nozzle (located at the injector plane) and a rectangular combustion chamber (110 × 110 mm^2). The test rig and measuring devices are shown schematically in Fig. 1. In the experiment, the length of the plenum L_p was 200–550 mm, so the air column length in the combustor was 1120–1670 mm. Combustion occurred in the chamber of 350 mm length equipped with sensor ports. The front quartz glass window provided optical access.

In the experiment, the range of the equivalence ratio Φ was 0.3–0.8. This is because lean combustion is prone to instability. As shown in Fig. 1, a siphon nozzle (Delavan, type SNA, P/N 30609-2) was clamped in the center of the swirler. The swirler was made by metal three-dimensional printing technology and had eight blades. The printing material was an aluminum alloy ($AlSi_{10}Mg$). The installation angle ψ of the blades was 60° or 75°, creating an azimuthal velocity component. The geometric swirl number S_n of the swirler could be calculated by:

$$S_n = \frac{2}{3}\left[\frac{1-(R_i/R_o)^3}{1-(R_i/R_o)^2}\right]\tan\psi \tag{1}$$

where R_i and R_o are the inner and outer radii of the primary air passage, respectively, and ψ is the vane installation angle (i.e., 60° or 75°). The S_n values for blade angles of 60° and 75° are 1.24 and 2.67, respectively.

Two float flowmeters adjusted the primary air and then sent the air into the plenum. A flow controller (Alicat Scientific, MCR series, 0–20 LPM) controlled the atomizing air flow rate (0.2 MPa, 10 L/min). The atomizing air sucked and sprayed the liquid fuel (10 mL/min) into the combustion chamber. The Sauter mean diameter (SMD) of the droplets produced by the injector in the steady state was $d_{SMD} \approx 40$ μm and the spray angle was 40°. The droplet size was determined using a particle dynamic analyzer (Dantec Dynamics A/S, FiberPDA) under non-reactive conditions. The physical properties of the ethanol and n-heptane fuels are shown in Table 1.

Table 1
Fuel properties of ethanol and n-heptane [35,37,38].

Parameter	Ethanol	n-Heptane
Purity	99.7% vol.	98.0% vol.
Molar mass [g/mol]	46.1	100.2
Dynamic viscosity (298.15 K) [mPa·s]	1.074	0.387
Density (298.15 K) [kg/m^3]	791	684
Lower calorific value [kJ/mol]	1365.5	4806.6
Boiling point [K]	351.6	371.6
Ignition temperature [K]	348.2	506.2

The complete combustion formulas of ethanol and n-heptane are given in Eqs. (2) and (3), respectively:

$$C_2H_5OH + 3O_2 \rightarrow 2CO_2 + 3H_2O \tag{2}$$

$$C_7H_{16} + 11O_2 \rightarrow 7CO_2 + 8H_2O \tag{3}$$

The calculated thermal power when burning ethanol and n-heptane were 3.9 and 5.5 kW, respectively.

A dynamic pressure sensor (Kunshan, CYG 1-406) was mounted on the chamber's back wall and located 5 mm downstream of the injector plane ($x = 0$ mm). A photomultiplier tube (PMT, Hamamatsu Photonics, H10722) coupled with a bandpass filter (centered at 430 ± 10 nm) was erected in front of the flame and kept a constant horizontal distance of 25 cm from the flame (Fig. 1). The PMT was used to measure the intensity of CH* chemiluminescence at the flame root representing the heat release rate of the flame, because the CH* chemiluminescence is proportional to the overall heat release rate for combustion mixtures, within certain limits [39]. The PMT was fixed 4 cm above the injector plane and almost received all the light passing through the combustion chamber window. The data acquisition device (National Instruments, USB-6210) sent the collected analog signals from the pressure transducer and PMT to a computer. A LabVIEW program controlled the

Table 2
Experimental conditions.

Parameter	Value
Theoretical thermal power $\overline{Q}$ [kW]	Ethanol: 3.9/n-heptane: 5.5
Equivalence ratio Φ	0.3–0.8 (step size of 0.05)
Plenum length L_p [mm]	200–550 (step size of 50)
Installation angle of the swirler blades ψ	60° ($S_n = 1.24$)/75° ($S_n = 2.67$)
Ambient temperature (K)	298–303
Environmental pressure (kPa)	101.3

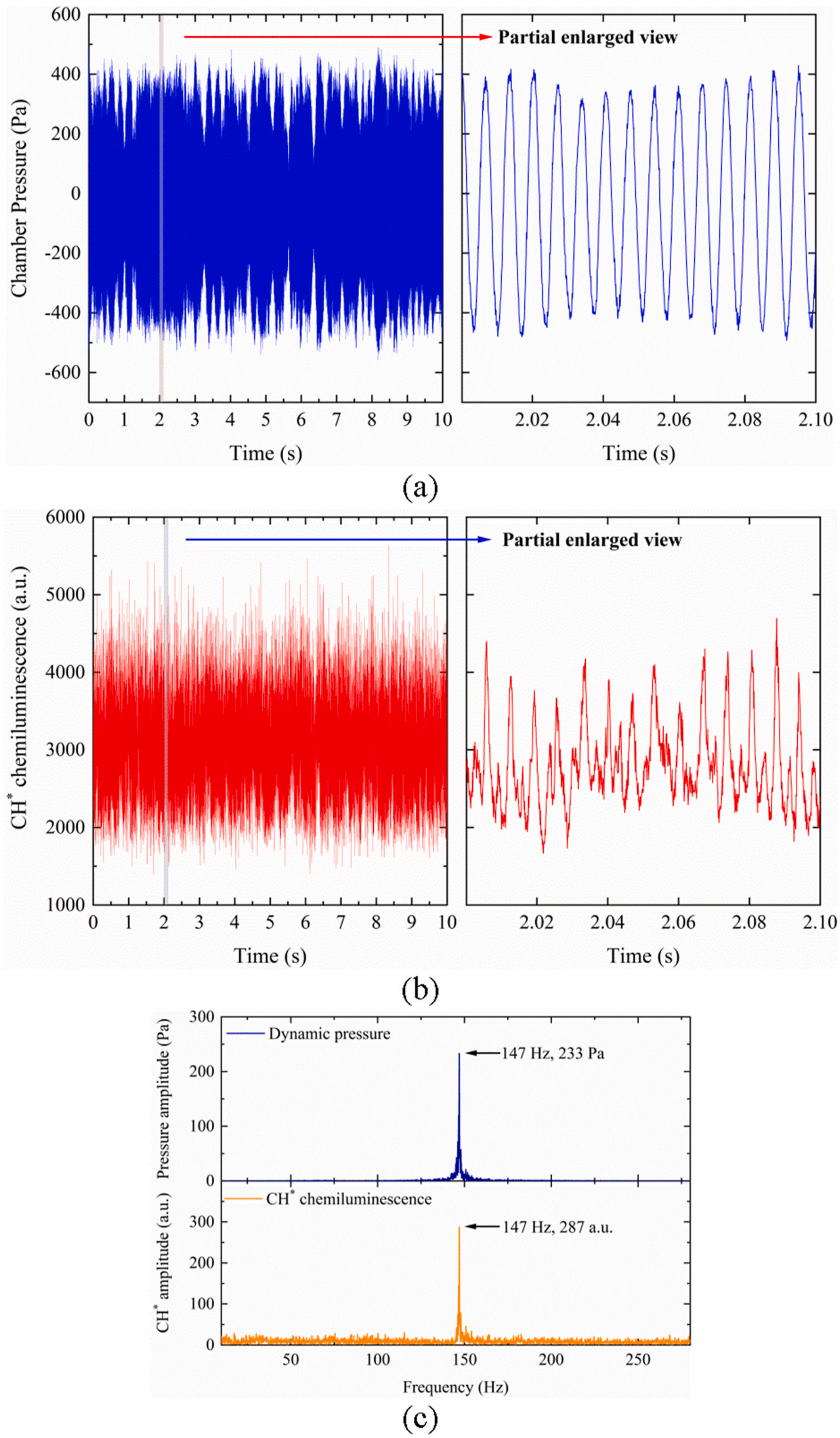

Fig. 2. Pulsation components of pressure and CH* chemiluminescence extracted by FFT (ethanol for combustion, $\psi = 60^{\circ}$, $L_p = 250$ mm and $\Phi = 0.35$): (a) 10 s pressure time signals; (b) 10 s CH* time signals; (c) FFT results of the signals.

experiment and managed the date for preprocessing. The sensor data were sampled synchronously at a frequency of 10 kHz for 10 s.

A K-type thermocouple thermometer (Apuhua TM-902C, 323–1573 K) was used to measure the fluid temperature at different axial heights in the combustor. A digital camera was used to capture instantaneous photographs of the flame and the frame rate was 30 fps. All experiments were carried out in a dark environment and were repeated two to five times. The air temperature and relative humidity were ~300 K and 60%, respectively. The experimental conditions are summarized in Table 2.

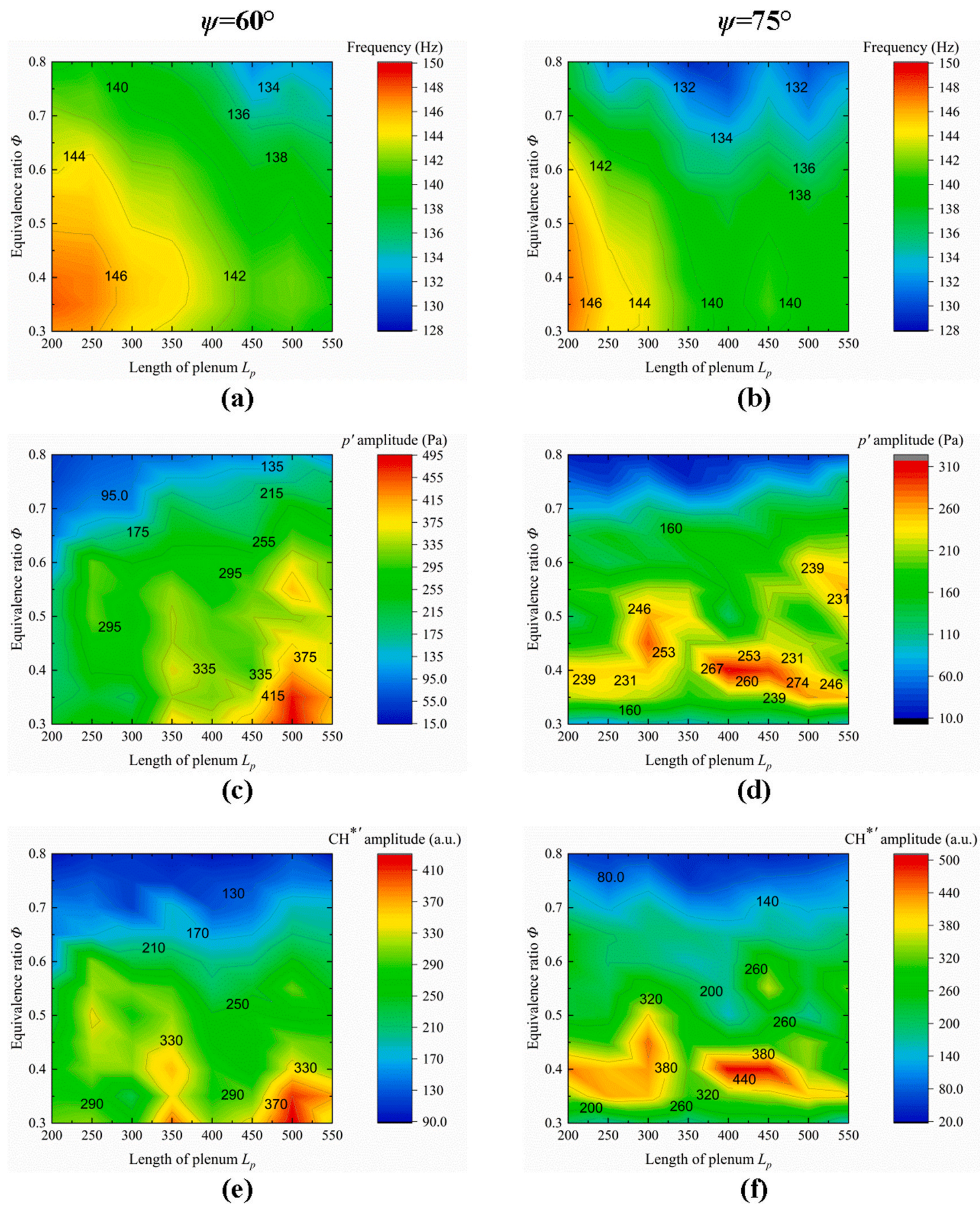

Fig. 3. Contour plots of (a, b) oscillation frequency, (c, d) pulsating pressure amplitude and (e, f) pulsating CH* amplitude as a function of the equivalence ratio Φ and the plenum length L_p for ethanol combustion. The corresponding swirler blade angles are 60° for the left column and 75° for the right column.

3. Result and discussion

3.1. Instability maps of ethanol swirling sprays

First, the intensity values of pulsating pressure and CH* chemiluminescence are obtained by fast Fourier transform (FFT). Fig. 2 shows the process of extracting the dynamic signal pulsation components when burning ethanol ($\psi = 60°$, $\Phi = 0.35$ and $L_p = 250$ mm). Fig. 2(a) shows the 10 s time series data of the pressure in the combustion chamber, while Fig. 2(c) shows the results of the FFT analysis of the pressure sensor and PMT signals. The phase contrast between the dynamic pressure and CH* chemiluminescence intensity signals is ignored because the phase difference is always less than 90° during oscillations [40].

Fig. 3 shows the contour plots of the oscillation frequency, pulsating pressure amplitude and the pulsating heat release rate as functions of the plenum length L_p and equivalence ratio Φ when ethanol is burned. According to the oscillation frequency contours (Fig. 3(a) and (b)), the oscillation frequency is 128–150 Hz.

The oscillation frequency is related to L_p and Φ. Fig. 3(a) and (b) show that as the Φ decreases, the oscillation frequency increases significantly. In addition, the longer the plenum length L_p, the lower the oscillation frequency. This is because the air column length in the combustor is increased, so the intrinsic frequency is lower.

According to Fig. 3(c), it can be seen that when the blade installation angle $\psi = 60°$, the amplitude of p' increases with decreasing Φ. This is because the flame length decreases as the Φ decreases first. The time delay is therefore reduced and the coupling degree between the

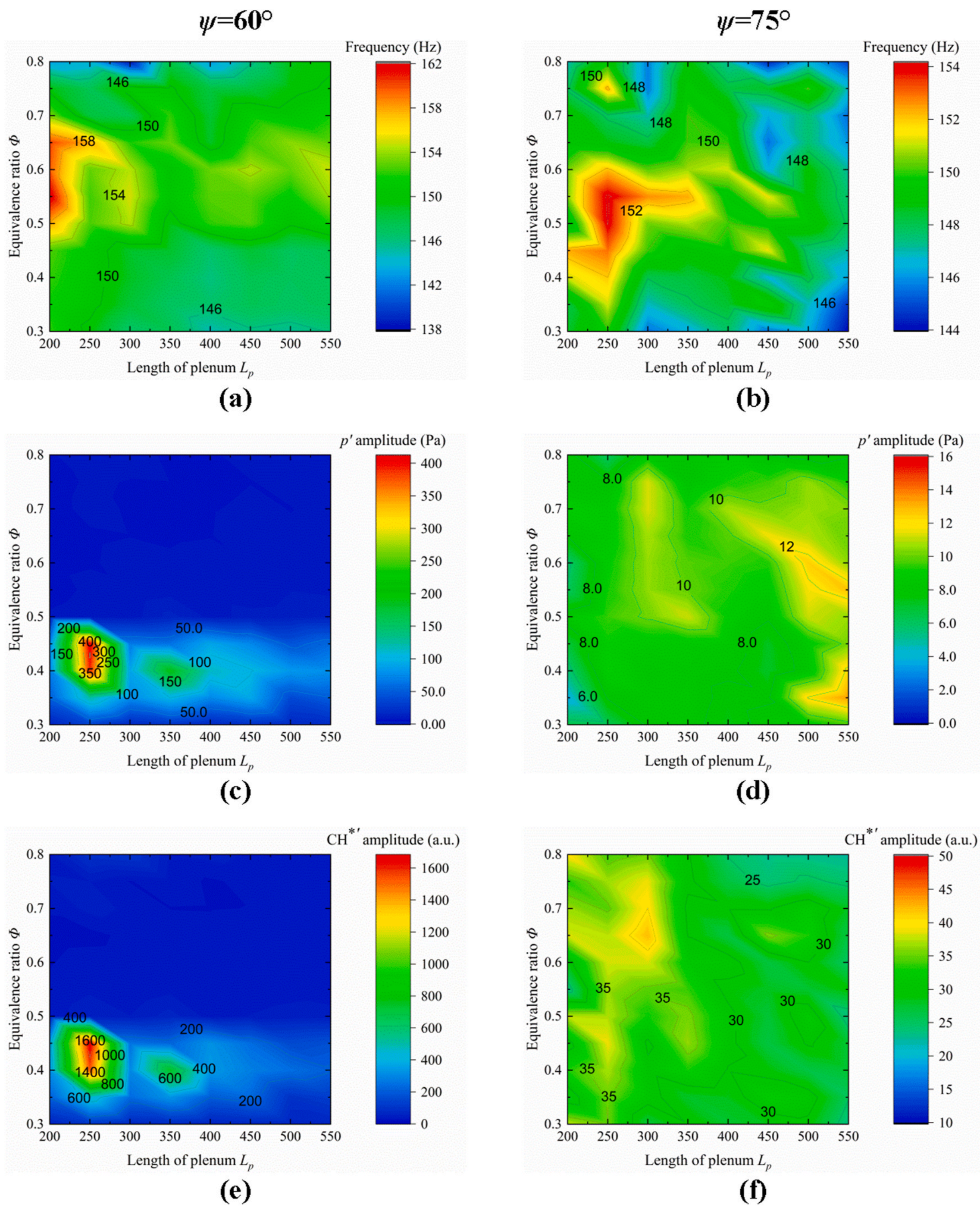

Fig. 4. Contour plots of (a, b) oscillation frequency, (c, d) pulsating pressure amplitude and (e, f) pulsating CH* amplitude as a function of the equivalence ratio Φ and the plenum length L_p for n-heptane combustion. The corresponding swirler blade angles are 60° for the left column and 75° for the right column.

pulsating heat release rate and the pulsating velocity is changed [41,42]. When $\Phi = 0.3$, the amplitude of p' reaches 495 Pa, i.e., 148 dB.

S_n may change the distribution of vortices. In particular, the position of the reaction zone may be changed, which in turn may cause the gain of the FTF to change. When $\psi = 75^\circ$, it can be seen from Fig. 3(d) that the stable range ($p' < 100$ Pa) is more extensive. When $\Phi > 0.7$, there is no significant pressure oscillation. Strong oscillations appear in the flame zone as the primary air flow rate increases (i.e., $\Phi\downarrow$). When $\Phi = 0.35$–0.45, the oscillation is most vigorous. The maximum amplitude of the pulsating pressure is ~310 Pa. When $\Phi < 0.35$, the pulsating pressure amplitude decreases instead. An earlier study conjectured that the drop of p' is mainly due to the nonlinear response of the swirling shear layer to the inlet velocity perturbations. The unstable airflow along the swirling shear layer changed the droplets' evaporation rate, flame distribution and kinetics [43]. When $\psi = 75^\circ$, the swirl number S_n is larger, so the sensitivity of the swirling shear layer to velocity perturbations is also different from that when $\psi = 60^\circ$. The maximum heat release plane moves downstream as the primary air increases (i.e., $\Phi\downarrow$) [44]. The amplitude of p' was found to decrease when $\Phi = 0.3$. Fig. 3(c) and (d) show that the plenum length also affects the amplitude of p' [45].

Comparing the amplitude contour plots of p' and CH*', it can be seen that the amplitude evolution of the pulsating heat release intensity is very similar to that of the pulsating pressure (Fig. 3(e) and (f)). This is because the p' and Q' are coupled and reinforce each other when combustion instability occurs. Therefore, when the amplitude of p' is high, the fluctuation of the heat release rate is also strong. The strong oscillation areas in Fig. 3(d) and (f) do not completely correspond. The reason for this difference remains to be studied.

3.2. Instability maps of n-heptane swirling sprays

The contours of the oscillation frequency and the amplitude of p' and CH*' are plotted in Fig. 4 when n-heptane fuel is burned. The frequency contours show that the oscillation frequency when burning n-heptane is ~5–10 Hz higher than that when burning ethanol. A reasonable explanation for this is that n-heptane has a higher calorific value than ethanol, which makes the overall temperature of the air column in the combustor higher, so the oscillation frequency increases slightly. This proves that the physical properties of the liquid fuel affect the oscillation frequency. The physical properties of the liquid fuel also have a strong influence on the instability amplitude (Fig. 4(c)–(f)). The stability range in the maps (e.g., p' amplitude below 100 Pa) is wider when n-heptane is burned.

Different from burning ethanol, when $\psi = 60°$, the oscillation frequency first increases and then decreases as Φ decreases. The reason for this oscillation frequency shift requires further research with knowledge of the FTF. The influence of L_p on the oscillation frequency is also different. Only when the equivalence ratio $\Phi = 0.45–0.75$ can it be observed that the shorter the plenum, the higher the oscillation frequency. When $\psi = 75°$, the oscillation frequency is less affected by Φ and L_p, which is ~144–154 Hz.

It can be seen from Fig. 4(c) and (e) that the stability margin of the combustor was significantly increased. When $\psi = 60°$, the pulsating pressure amplitude increases slowly with decreasing equivalence ratio (Fig. 4(c)). When Φ decreases to 0.5, the amplitude of p' starts to increase. With $\Phi < 0.35$, the amplitude decreases again. This is similar to the pattern shown in Fig. 3(d).

The length of the plenum also has a significant effect on the amplitude of p'. When $L_p = 250$ mm, strong pressure oscillations occur in the combustion chamber. In particular, when $\Phi = 0.40–0.45$, the amplitude of p' is close to 415 Pa. The vibration of the air column even caused the structural oscillation of the experimental bench. The amplitude contours of CH*' show a similar pattern. When $\Phi = 0.40–0.45$ and $L_p = 250$ mm, the pulsating CH* luminosity even exceeds 1600 a.u., which is three times that when burning ethanol. The excessive increase in CH*' amplitude appears to be related to fuel properties. Figs. 3–4 show that the effect of plenum length on the amplitude of p' is different for different fuels, which is related to the flame structure and requires further analysis using FTF.

When the blade installation angle $\psi = 75°$, the amplitude of the pulsating pressure and the pulsating heat release rate are significantly reduced and the maximum values do not exceed 15 Pa and 45 a.u., respectively. This shows that when $\psi = 75°$, Φ or L_p has less effect on the combustion stability and the safety range available for operation is larger. Fig. 4(c) and (d) show that ψ can affect the degree of combustion instability [25]. This is similar to the situation when burning ethanol, the mechanism has been discussed above.

In order to further analyze the influence of ψ and the physical properties of the liquid fuels on combustion stabilities, eight typical operating cases were selected for comparison, namely, ethanol or n-heptane fuel, Φ is 0.35 or 0.75 and ψ is 60° or 75°. The L_p is fixed at 250 mm.

It can be seen from Figs. 3 and 4 that when $\Phi = 0.35$ and $\psi = 60°$, the pulsating pressure amplitude during ethanol combustion is ~220 Pa and the pulsating heat release rate amplitude exceeds 280 a.u. The amplitudes of p' and CH*' during n-heptane combustion are 122 Pa and 462 a.u, respectively. When Φ increases to 0.75, the oscillation weakens, the p' amplitude during ethanol combustion drops to 83 Pa and the amplitude of CH*' is only 130 a.u. When n-heptane is burned, the amplitudes of the pulsating pressure and heat release rate drop to 7 Pa and 40 a.u., respectively.

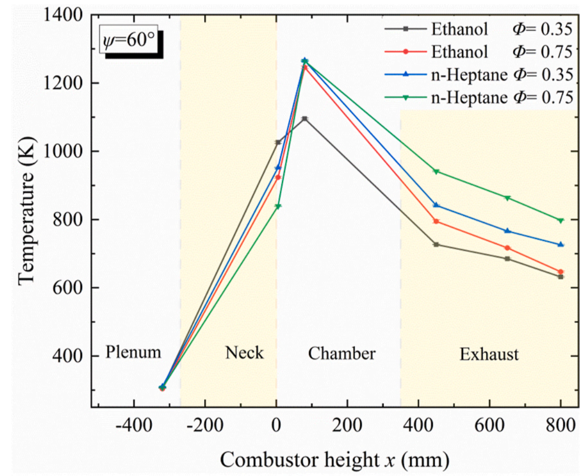

(a)

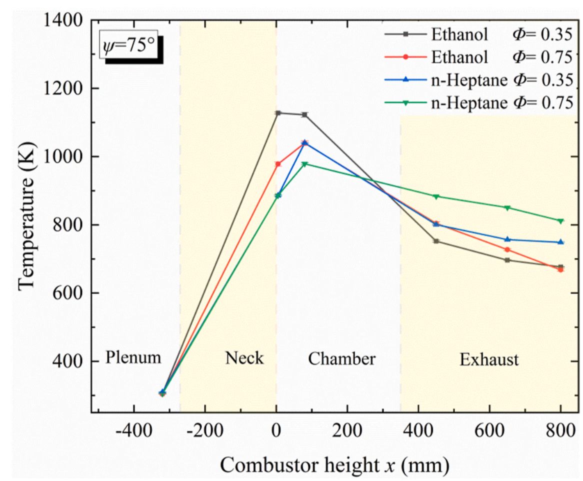

(b)

Fig. 5. The temperature of the flow field inside the combustor when (a) $\psi = 60°$ and (b) $\psi = 75°$.

When $\psi = 75°$, the amplitude of the pulsating pressure and heat release rate show similar patterns to those at $\psi = 60°$ for ethanol fuel. However, the n-heptane combustion instability almost disappears when $\psi = 75°$. The pulsating pressure amplitude does not exceed 20 Pa regardless of the equivalence ratio and the heat release pulsation almost disappears. Under these eight combustion conditions, the temperature measurement results at different axial heights of the combustor are shown in Sect. 3.3.

3.3. Temperature distribution and flame shape analysis

The temperature measurement results show that the local temperature at the flame root ($x = 5$ mm) is higher when Φ is lower (Fig. 5). This is because the smaller the equivalent ratio, the more thoroughly the fuel burns at the flame root. The turbulence effect enhances the mixing of vaporized droplets and oxidant, enhances combustion and shortens the flame length, thereby reducing the range of spray combustion and increasing the flame root temperature. In addition, when the air flow rate increases, excessive air dilution and convection will cause more heat loss, thereby reducing the brightness and length of the flame [42]. Regardless of the fuel type and vane angle, the temperature always conforms to this rule.

According to the axial temperature distribution, the lower the equivalence ratio, the lower the temperature in the exhaust section. This is because the lower Φ means that more low-temperature primary air is

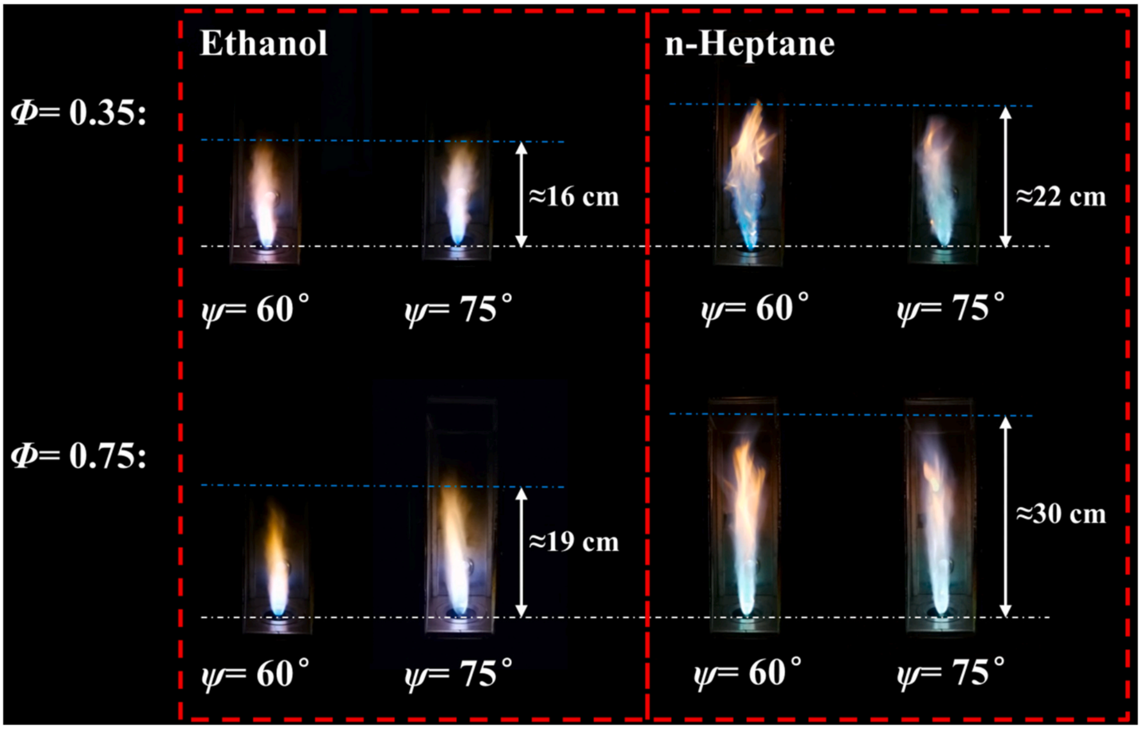

Fig. 6. Instantaneous flame photographs of ethanol (left) and n-heptane (right). The equivalence ratios for the upper and lower rows are 0.35 and 0.75, respectively.

supplied into the combustor. Heat is quickly taken away from the combustor by thermal convection, so the temperature drops. In addition, it can be inferred that the exhaust section temperature when burning n-heptane is significantly higher than that when burning ethanol. The flue gas in the exhaust section is heated by the n-heptane flame tail, which is confirmed by the flame snapshots (Fig. 6). This is because the n-heptane flame is longer, which may be related to its higher boiling and ignition temperature (see Table 1) and longer carbon chain. In addition, the ethanol molecule contains oxygen, which also contributes to shortening the flame length [42].

The temperature measurements also show that the root temperature is much higher for the strongly oscillating ethanol flame than the n-heptane flame. In the exhaust section, the temperature is much lower when burning ethanol than when burning n-heptane. The temperature curves show that the temperature at the flame root ($x = 5$ mm) is ranked as T(ethanol, $\Phi = 0.35$) > T(ethanol, $\Phi = 0.75$) > T(n-heptane, $\Phi = 0.35$) > T(n-heptane, $\Phi = 0.75$). The temperature ranking of the exhaust section ($x > 350$ mm) is T(ethanol, $\Phi = 0.35$) < T(ethanol, $\Phi = 0.75$) < T (n-heptane, $\Phi = 0.35$) < T(n-heptane, $\Phi = 0.75$). The pulsating pressure amplitude ranking is p' (ethanol, $\Phi = 0.35$) > p' (ethanol, $\Phi = 0.75$) > p' (n-heptane, $\Phi = 0.35$) > p' (n-heptane, $\Phi = 0.75$).

The temperature distribution appears to be correlated with the amplitude of the pulsating pressure. The oscillations are more pronounced when the flame root temperature is high and the exhaust section temperature is low. This indicates that the oscillation may be related to the uneven temperature distribution in the combustor. The greater the difference in temperature at different heights of the combustor, the more pronounced the oscillation. The different physical properties of the fuel cause the difference in temperature distribution and combustion stability. When burning ethanol, the reaction zone is more compact and the temperature gradient of the flow field in the combustor along the x-axis is larger, which is one of the crucial reasons for the formation of pressure waves. A previous study has also shown that the chemical properties of the fuel are related to ignition delay and flame temperature [33]. The physical properties of the fuel also affect the penetration ability and evaporation life of the spray droplets, which are related to the reaction intensity [46]. The influence of the chemical reaction characteristics of different fuels on combustion instability and the causal relationship between temperature distribution and system stability need to be further studied.

From the flame transient photographs, it can be seen that the n-heptane flame is longer than the ethanol flame and the effect of the blade angle on the flame length is not very obvious, but the effect of the equivalent ratio on the flame length is noticeable (Fig. 6). When the Φ increased from 0.35 to 0.75, the ethanol flame height increased from 16 to 19 cm and the flame length of n-heptane increased from 22 to 30 cm. The differences in flame size and temperature distribution caused by differences in fuel properties may potentially be related to the strength of thermoacoustic oscillations [47]. The influence of the blade angle on the oscillation intensity is more subtle. Although the flame length does not change much under different blade angles, the change of the swirl intensity may still cause the change of the instantaneous flame surface. A high-speed PLIF or a high-speed camera equipped with an image intensifier (ICCD) is required to observe the rapid changes of perturbed-flame shape with shorter exposure times [43,48,49]. It should be emphasized that thermoacoustic oscillations are not only related to flame macrostructure. Shorter flame simply reflects its greater tendency to generate combustion oscillations.

4. Conclusions

Lean combustion systems are prone to spontaneous combustion instabilities, which has become a challenging issue for developing lean combustion technologies. Combustion instabilities may cause combustor vibration and loud noises, induce flame quenching and flashback and severely damage the combustor components. In order to gain insight into the mechanism of combustion instability of liquid fuels and explore the effects of burner structure, equivalence ratio and fuel properties on combustion stability, combustion instability maps were drawn for ethanol and n-heptane. Some important conclusions are presented below.

When burning ethanol, the oscillation frequency increases with decreasing equivalence ratio and plenum length. When the equivalence ratio is lower than 0.7, the amplitudes of the pulsating pressure and heat release rate increase significantly. The stable combustion range of n-heptane is wider, revealing that the fuel's physical properties affect the combustion stability. The equivalence ratio and the plenum length also affect the amplitude of the pulsating pressure and heat release rate. When the plenum length is 250 mm and the equivalence ratio is 0.40–0.45, the pulsating pressure amplitude is close to 415 Pa when burning n-heptane. The pulsating CH* chemiluminescence intensity even exceeds 1600 a.u., which is three times higher than the pulsating CH* intensity when burning ethanol. The intense pressure fluctuations even caused structural vibrations in the model combustor.

Further studies confirmed that the different fuel properties resulted in different flame structure and temperature distribution in the combustor, which may be one of the potential reasons for the different combustion stability performance between ethanol and n-heptane. Ethanol flames are shorter and more compact and appear to be more prone to combustion instability. In future studies, large eddy simulation and more accurate combustion diagnosis methods will be applied to verify the decisive influence of flame size and temperature distribution on combustion stabilities.

Declaration of competing interest

The authors declare that they have no known competing financial interests or personal relationships that could have appeared to influence the work reported in this paper.

Acknowledgment

This research was supported by the National Science Fund for Distinguished Young Scholars [grant number, 51825605]. We thank International Science Editing for editing this manuscript.

References

[1] Y. Huang, V. Yang, Dynamics and stability of lean-premixed swirl-stabilized combustion, Prog. Energy Combust. Sci. 35 (2009) 293–364, https://doi.org/10.1016/j.pecs.2009.01.002.
[2] Rayleigh, The explanation of certain acoustical phenomena, Nature 18 (1878) 319–321, https://doi.org/10.1038/018319a0.
[3] Z.X. Chen, N. Swaminathan, Influence of fuel plenum on thermoacoustic oscillations inside a swirl combustor, Fuel 275 (2020), 117868, https://doi.org/10.1016/j.fuel.2020.117868.
[4] T. Poinsot, Prediction and control of combustion instabilities in real engines, Proc. Combust. Inst. 36 (2017) 1–28, https://doi.org/10.1016/j.proci.2016.05.007.
[5] Y. Liu, J. Li, T. Zhang, Y. Yan, Active suppression of swirl-stabilized combustion instability, Fuel 287 (2021), 119559, https://doi.org/10.1016/j.fuel.2020.119559.
[6] A. Ghani, T. Steinbacher, A. Albayrak, W. Polifke, Intrinsic thermoacoustic feedback loop in turbulent spray flames, Combust. Flame 205 (2019) 22–32, https://doi.org/10.1016/j.combustflame.2019.03.039.
[7] E.C. Okafor, H. Yamashita, A. Hayakawa, K.D.K.A. Somarathne, T. Kudo, T. Tsujimura, M. Uchida, S. Ito, H. Kobayashi, Flame stability and emissions characteristics of liquid ammonia spray co-fired with methane in a single stage swirl combustor, Fuel 287 (2021), 119433, https://doi.org/10.1016/j.fuel.2020.119433.
[8] S. Candel, D. Durox, T. Schuller, P. Palies, J.F. Bourgouin, J.P. Moeck, Progress and challenges in swirling flame dynamics, Compt. Rendus Mec. 340 (2012) 758–768, https://doi.org/10.1016/j.crme.2012.10.024.
[9] D. Zhao, Z. Lu, H. Zhao, X.Y. Li, B. Wang, P. Liu, A review of active control approaches in stabilizing combustion systems in aerospace industry, Prog. Aero. Sci. 97 (2018) 35–60, https://doi.org/10.1016/j.paerosci.2018.01.002.
[10] D. Zhao, J. Li, Feedback control of combustion instabilities using a helmholtz resonator with an oscillating volume, Combust. Sci. Technol. 184 (2012) 694–716, https://doi.org/10.1080/00102202.2012.660224.
[11] D. Yang, A.S. Morgans, A semi-analytical model for the acoustic impedance of finite length circular holes with mean flow, J. Sound Vib. 384 (2016) 294–311, https://doi.org/10.1016/j.jsv.2016.08.006.
[12] D. Yang, X. Wang, M. Zhu, The impact of the neck material on the sound absorption performance of Helmholtz resonators, J. Sound Vib. 333 (2014) 6843–6857, https://doi.org/10.1016/j.jsv.2014.07.034.
[13] S. Li, Y. Zheng, M. Zhu, D.M. Martinez, X. Jiang, Large-eddy simulation of flow and combustion dynamics in a lean partially premixed swirling combustor, J. Energy Inst. 90 (2017) 120–131, https://doi.org/10.1016/j.joei.2015.09.004.
[14] P. Palies, D. Durox, T. Schuller, S. Candel, Nonlinear combustion instability analysis based on the flame describing function applied to turbulent premixed swirling flames, Combust. Flame 158 (2011) 1980–1991, https://doi.org/10.1016/j.combustflame.2011.02.012.
[15] M. Nemitallah, S. Alkhaldi, A. Abdelhafez, M. Habib, Effect analysis on the macrostructure and static stability limits of oxy-methane flames in a premixed swirl combustor, Energy 159 (2018) 86–96, https://doi.org/10.1016/j.energy.2018.06.131.
[16] R.M. Gejji, C. Huang, C. Fugger, C. Yoon, W. Anderson, Parametric investigation of combustion instabilities in a single-element lean direct injection combustor, Int. J. Spray Combust. Dyn. 11 (2019) 1–16, https://doi.org/10.1177/1756827718785851.
[17] B. Ahn, J. Lee, S. Jung, K.T. Kim, Low-frequency combustion instabilities of an airblast swirl injector in a liquid-fuel combustor, Combust. Flame 196 (2018) 424–438, https://doi.org/10.1016/j.combustflame.2018.06.031.
[18] T. Lee, J. Lee, J. Park, D. Han, K. Tae, Staggered swirler arrangement in two self-excited interacting swirl flames, Combust. Flame 198 (2018) 363–375, https://doi.org/10.1016/j.combustflame.2018.10.001.
[19] J. Yoon, M.K. Kim, J. Hwang, J. Lee, Y. Yoon, Effect of fuel-air mixture velocity on combustion instability of a model gas turbine combustor, Appl. Therm. Eng. 54 (2013) 92–101, https://doi.org/10.1016/j.applthermaleng.2013.01.032.
[20] L. Xu, J. Zheng, G. Wang, Z. Feng, X. Tian, L. Li, F. Qi, Investigation on the intrinsic thermoacoustic instability of a lean-premixed swirl combustor with an acoustic liner, Proc. Combust. Inst. 38 (2021) 6095–6103, https://doi.org/10.1016/j.proci.2020.06.155.
[21] Z. Rao, R. Li, B. Zhang, B. Wang, D. Zhao, M.S. Akhtar, Experimental investigations of equivalence ratio effect on nonlinear dynamics features in premixed swirl-stabilized combustor, Aero. Sci. Technol. 112 (2021), 106601, https://doi.org/10.1016/j.ast.2021.106601.
[22] Z.X. Chen, N. Swaminathan, M. Stöhr, W. Meier, Interaction between self-excited oscillations and fuel-air mixing in a dual swirl combustor, Proc. Combust. Inst. 37 (2019) 2325–2333, https://doi.org/10.1016/j.proci.2018.08.042.
[23] E. Lo Schiavo, D. Laera, E. Riber, L. Gicquel, T. Poinsot, Effects of liquid fuel/wall interaction on thermoacoustic instabilities in swirling spray flames, Combust. Flame 219 (2020) 86–101, https://doi.org/10.1016/j.combustflame.2020.04.015.
[24] Y. Tongxun, D.A. Santavicca, Combustion instability in a turbulent liquid-fueled swirl-stabilized LDI combustor, in: 45th AIAA/ASME/SAE/ASEE Jt. Propuls. Conf. Exhib, 2009, https://doi.org/10.2514/6.2009-5014.
[25] D. Durox, J.P. Moeck, J.F. Bourgouin, P. Morenton, M. Viallon, T. Schuller, S. Candel, Flame dynamics of a variable swirl number system and instability control, Combust. Flame 160 (2013) 1729–1742, https://doi.org/10.1016/j.combustflame.2013.03.004.
[26] B. Zhang, M. Shahsavari, Z. Rao, S. Yang, B. Wang, Thermoacoustic instability drivers and mode transitions in a lean premixed methane-air combustor at various swirl intensities, Proc. Combust. Inst. 38 (2021) 6115–6124, https://doi.org/10.1016/j.proci.2020.06.226.
[27] C. Ruan, F. Chen, T. Yu, W. Cai, Y. Mao, Y. Qian, X. Li, X. Lu, Experimental study on combustion stability characteristics in liquid-fueled gas turbine model combustor: fuel sensitivities and flame/flow dynamics, Fuel 265 (2020), 116973, https://doi.org/10.1016/j.fuel.2019.116973.
[28] D. Kim, J. Martz, A. Violi, Effects of fuel physical properties on direct injection spray and ignition behavior, Fuel 180 (2016) 481–496, https://doi.org/10.1016/j.fuel.2016.03.085.
[29] P. Rajendram Soundararajan, G. Vignat, D. Durox, A. Renaud, S. Candel, Effect of different fuels on combustion instabilities in an annular combustor, J. Eng. Gas Turbines Power 143 (2021), 031007, https://doi.org/10.1115/1.4049702.
[30] E. Karlis, Y. Hardalupas, A.M.K.P. Taylor, Effects of inert fuel diluents on thermoacoustic instabilities in gas turbine combustion, AIAA J. 58 (2020) 2643–2657, https://doi.org/10.2514/1.J058312.
[31] R.L. Speth, A.F. Ghoniem, Using a strained flame model to collapse dynamic mode data in a swirl-stabilized syngas combustor, Proc. Combust. Inst. 32 II (2009) 2993–3000, https://doi.org/10.1016/j.proci.2008.05.072.
[32] J. Li, Y. Xia, A.S. Morgans, X. Han, Numerical prediction of combustion instability limit cycle oscillations for a combustor with a long flame, Combust. Flame 185 (2017) 28–43, https://doi.org/10.1016/j.combustflame.2017.06.018.
[33] X. Fu, S.K. Aggarwal, Fuel unsaturation effects on NOx and PAH formation in spray flames, Fuel 160 (2015) 1–15, https://doi.org/10.1016/j.fuel.2015.07.075.
[34] F. Maroteaux, B.M. Vaglieco, E. Mancaruso, N-heptane ignition delay time with temperature criterion for HCCI combustion, Fuel 225 (2018) 483–489, https://doi.org/10.1016/j.fuel.2018.03.182.
[35] C. Jin, X. Zhang, Z. Geng, X. Pang, X. Wang, J. Ji, G. Wang, H. Liu, Effects of various co-solvents on the solubility between blends of soybean oil with either methanol or ethanol, Fuel 244 (2019) 461–471, https://doi.org/10.1016/j.fuel.2019.01.187.
[36] Z. Zheng, L. Yue, H. Liu, Y. Zhu, X. Zhong, M. Yao, Effect of two-stage injection on combustion and emissions under high EGR rate on a diesel engine by fueling blends of diesel/gasoline, diesel/n-butanol, diesel/gasoline/n-butanol and pure diesel, Energy Convers. Manag. 90 (2015) 1–11, https://doi.org/10.1016/j.enconman.2014.11.011.
[37] I. Pielecha, S. Wierzbicki, M. Sidorowicz, D. Pietras, Combustion thermodynamics of ethanol, n-heptane, and n-butanol in a rapid compression machine with a dual direct injection (DDI) supply system, Energies 14 (2021), https://doi.org/10.3390/en14092729.
[38] A. Böğrek, C. Haşimoğlu, A. Calam, B. Aydoğan, Effects of n-heptane/toluene/ethanol ternary fuel blends on combustion, operating range and emissions in premixed low temperature combustion, Fuel 295 (2021), https://doi.org/10.1016/j.fuel.2021.120628.
[39] N.N. Deshmukh, S.D. Sharma, Suppression of thermo-acoustic instability using air injection in horizontal Rijke tube, J. Energy Inst. 90 (2017) 485–495, https://doi.org/10.1016/j.joei.2016.03.001.

[40] H. Zhou, Z. Liu, C. Tao, M. Zhou, Passive suppression of self-excited combustion instabilities in liquid spray flame using microperforated plate, J. Eng. Gas Turbines Power 142 (2020), 111013, https://doi.org/10.1115/1.4047768.

[41] P.R. Alemela, D. Fanaca, C. Hirsch, T. Sattelmayer, B. Schuermans, Determination and scaling of thermo acoustic characteristics of premixed flames, Int. J. Spray Combust. Dyn. 2 (2010) 169–198, https://doi.org/10.1260/1756-8277.2.2.169.

[42] S.I. Yang, M.S. Wu, T.C. Hsu, Spray combustion characteristics of kerosene/bio-oil part I: experimental study, Energy 119 (2017) 26–36, https://doi.org/10.1016/j.energy.2016.12.062.

[43] T. Yi, D.A. Santavicca, Combustion instability and flame structure of turbulent swirl-stabilized liquid-fueled combustion, J. Propul. Power 28 (2012) 1000–1014, https://doi.org/10.2514/1.B34438.

[44] K. Wang, F. Li, P. Zou, X. Lin, R. Mao, X. Yu, Effect of the fuel-air flow velocity on heat release rate of swirling non-premixed methane flames, Aero. Sci. Technol. 95 (2019), 105465, https://doi.org/10.1016/j.ast.2019.105465.

[45] H. Zhou, Z. Liu, C. Tao, M. Zhou, Mitigating self-excited thermoacoustic oscillations in a liquid fuel combustor using dual perforated plates, J. Acoust. Soc. Am. 148 (2020) 1756–1766, https://doi.org/10.1121/10.0002007.

[46] C.T. Chong, S. Hochgreb, Spray flame structure of rapeseed biodiesel and Jet-A1 fuel, Fuel 115 (2014) 551–558, https://doi.org/10.1016/j.fuel.2013.07.059.

[47] F. Li, M. Du, L. Yang, Effect of fuel injection parameters on performance characteristics and emissions of a thermoacoustic system, Aero. Sci. Technol. 110 (2021), 106512, https://doi.org/10.1016/j.ast.2021.106512.

[48] H. Liu, Y. Cui, B. Chen, D.C. Kyritsis, Q. Tang, L. Feng, Y. Wang, Z. Li, C. Geng, M. Yao, Effects of flame temperature on PAHs and soot evolution in partially premixed and diffusion flames of a diesel surrogate, Energy Fuel. 33 (2019) 11821–11829, https://doi.org/10.1021/acs.energyfuels.9b02315.

[49] X. Han, D. Laera, A.S. Morgans, C.J. Sung, X. Hui, Y.Z. Lin, Flame macrostructures and thermoacoustic instabilities in stratified swirling flames, Proc. Combust. Inst. 37 (2019) 5377–5384, https://doi.org/10.1016/j.proci.2018.06.147.